Carbohydrate Polymers 349 (2025) 122940

Contents lists available at ScienceDirect

Carbohydrate Polymers

journal homepage: www.elsevier.com/locate/carbpol

Characterization of hemicellulose in sacred lotus (*Nelumbo nucifera* Gaetn.) petiole during xylogenesis

Anran Feng [a], Yingying Guan [b,c], Haoqiang Yang [b,c], Biao Zheng [b,c], Wei Zeng [e], Pengfei Hao [e], Antony Bacic [e], Shi-you Ding [a,*], Ai-min Wu [b,c,d,**]

[a] *Plant Biology Department, Michigan State University, East Lansing, MI 48824, USA*
[b] *State Key Laboratory for Conservation and Utilization of Subtropical Agro-bioresources, Guangzhou 510642, China*
[c] *Guangdong Key Laboratory for Innovative Development and Utilization of Forest Plant Germplasm, College of Forestry and Landscape Architectures, South China Agricultural University, Guangzhou 510642, China*
[d] *Guangdong Laboratory of Lingnan Modern Agriculture, Guangzhou 510642, China*
[e] *La Trobe Institute for Sustainable Agriculture and Food, School of Life Sciences, La Trobe University, Bundoora, VIC 3086, Australia*

ARTICLE INFO

Keywords:
Hemicellulose
2D HSQC NMR
Xylogenesis
Nelumbo nucifera
Petiole

ABSTRACT

Hemicelluloses play a crucial role in connecting cellulose and lignin within the plant cell wall and find extensive biotechnological applications. There is a notable gap in research concerning the hemicellulose from *Nelumbo nucifera*, the basal eudicot adapted to aquatic environments. To fill this gap, hemicellulose characteristics from the apical to the basal segments of petioles from 4-month-old *N. nucifera* plants were examined. Results showed that during the initial phase of xylogenesis, xyloglucan predominated in the hemicellulose fraction, while later stages were gradually dominated by 4-*O*-methyl-D-glucurono-D-xylan (MGX). Having a typical tetrasaccharide reducing end, the glucuronoxylan in *N. nucifera* was also shown with a typical the MeGlcA on the C2 Xyl carbon sidechain. The total degree of acetylation increased from apex (0.45) to base (0.55) of petiole. Notably, no arabinosyl side-chains were detected in the *N. nucifera* xylan, suggesting that *N. nucifera* hemicellulose aligns most closely with dicot wood rather than the non-commelinid monocot (grass). Transcriptomic analysis also indicated that the middle and basal region exhibited higher xylan synthesis activity. This study contributes new evidence supporting the conservation of dicotyledonous hemicellulose during evolution.

1. Introduction

Hemicelluloses are one of the major components of the plant cell wall, comprising approximately 20–35 % of the plant biomass (by dry weight). While cellulose is the major load-bearing component of the cell wall, cellulose microfibrils are connected to hemicellulose by both covalent and non-covalent linkages, and this connection is an important component in the regulation of the cell wall structure. It is also worth noting that the hemicelluloses, especially their functional group derivatives, are of great biotechnological value/potential, such as industrial applications in the production of packaging film (Hansen & Plackett, 2008), hydrogel for drug delivery (Xu et al., 2023), or emulsifiers for food (Wang et al., 2017). In addition, hemicelluloses can be hydrolyzed to their monosaccharides and these can be then converted to derivatives such as furfural, which is produced by the dehydration of xylose (Xyl) and arabinose (Ara), serving as a platform chemical for a wide range of downstream applications (Eseyin & Steele, 2015).

From the chemical perspective, hemicelluloses are a heterogeneous group of polysaccharides with β-(1 → 4)-linked backbones of glucose (Glc), mannose (Man), or xylose (Xyl) (Scheller & Ulvskov, 2010). Hemicellulose composition and properties are markedly different among dicotyledons, non-commelinid monocots(grasses), and gymnosperms/conifers as well as between the primary and the secondary cell walls (SCW). Hemicelluloses in the primary cell wall, especially in dicots, are predominantly xyloglucans (XyG or XG) which consists of a β-(1 → 4)-linked Glc backbone, with sing Xyl or Xyl-based side chains containing Ara, Gal, and/or fucosyl (Fuc) units. XGs are present in every land plant ever examined but are not found in the freshwater green algae, the Charophytes (Popper, 2008). Hemicelluloses containing Man can be grouped into different classes of heteromannans, including

* Corresponding author.
** Correspondence to: A. Wu, State Key Laboratory for Conservation and Utilization of Subtropical Agro-bioresources, Guangzhou 510642, China.
E-mail addresses: sding@msu.edu (S.-y. Ding), wuaimin@scau.edu.cn (A.-m. Wu).

https://doi.org/10.1016/j.carbpol.2024.122940
Received 25 October 2024; Accepted 31 October 2024
Available online 8 November 2024

mannans or glucomannans on the basis of whether Glc is present in their backbone, and they can be further modified to galactomannan or galactoglucomannan (GGM) at the C5 position of the Man backbone, with a Gal residue. Galactoglucomannan is the major hemicellulose of the SCW of gymnosperms (Capek et al., 2000). Xylan is the general term for polysaccharides composed of β-(1 → 4)-linked Xyl as the backbone. In the SCWs of dicots, xylan is usually modified with 4-*O*-methyl-α-D-glucuronic acid residues (MeGlcA) or its non-methylated form (GlcA) at the C2 of Xyl*p* units, resulting in them also being known as 4-*O*-methyl-D-glucurono-D-xylans (MGX) or glucuronoxylans (GX). But in the commelinid monocots, in which the primary cell walls contain ferulic acid, xylan also contains a high proportion of Ara*f* residues and is known as glucuronoarabinoxylans (GAX). Interestingly, some exceptions exist for dicotyledonous xylan with abundant Ara*f* substitution, such as in the sycamore primary walls (Darvill et al., 1980), the seed mucilage of flax (Naran et al., 2008), the leaves of *A. thaliana* (Zablackis et al., 1995) and the psyllium seeds (Fischer et al., 2004). The O2 and O3 positions of most xylans are often *O*-acetylated to various degrees (Ebringerová et al., 2005). The acetylation of xylan is crucial for the accumulation and structural formation of the SCWs by *TBLs* (Yuan et al., 2016). Acetylation plays a role in defending against microbial invasion by conferring a significant resistance to the enzymatic degradation (Sista Kameshwar & Qin, 2018).

The biosynthesis of the hemicellulose has been under intense research for decades. Although the exact mechanism is unclear, the biosynthesis of xylan is suggested to be initiated by three possibilities: *de novo* initiation, using a xylooligomer or using the tetrasaccharide sequence (β-Xyl-(1,3)-α-Rha-(1,2)-α-GalA-(1,4)-Xyl) at the reducing end as a primer (Wang et al., 2022; Ye & Zhong, 2022). Four genes from Arabidopsis were identified genetically as being involved in the synthesis of the tetrasaccharide sequence — namely *PARVUS*, *IRX8*, *FRA9* and *FRA8/F8H* (Lee et al., 2007, 2009; Ye & Zhong, 2022). The elongation of the backbone of xylan is implemented by the synergistical cooperation of three groups of glycosyltransferases (GTs), *AtIRX10/10L*, *AtIRX9/9L*, and *AtIRX14/14L* (Brown et al., 2007; Jiang et al., 2016; Wu et al., 2009, 2010; Zeng et al., 2016). Methylation at the O4 of GlcA residues is catalyzed by DUF579 domain-containing protein GXMs (Lee, Teng, Zhong, Yuan, et al., 2012; Urbanowicz et al., 2012). The Xylp: MeGlcA ratio ranges from 4:1 to 16:1 for typical hardwoods (Ebringerová et al., 2005). The percentage of 4-*O*-methylated GlcA is dependent upon the source species, as 60 % of the GlcA are methylated in Arabidopsis while all GlcA are methylated in *Populus* (Lee et al., 2011; Yuan et al., 2014). GlcA residues are transferred to the xylan backbone by GUX1/2/3 proteins with UDP-GlcA the donor (Lee, Teng, Zhong, & Ye, 2012; Mortimer et al., 2010). In terms of xyloglucan biosynthesis, the genes responsible for the backbone elongation were first identified in nasturtium seeds as CSLC (cellulose synthase like-C), and later validated by quintuple mutations in Arabidopsis (Cocuron et al., 2007; Kim et al., 2020). As described above, the synthesis of hemicellulose is a complicated cellular process regulated by a series of agents across the secretory pathway to the cell wall.

Xylogenesis is the process of the maturation of xylem. During this process, the hemicellulose composition and structure usually undergoes certain changes. Previous studies of xylogenesis on various plant species have shown different patterns of hemicellulose dynamics. The hemicellulose composition in *Cunninghamia lanceolata*, a gymnosperm softwood, undergoes a steady increase in GGM and a gradual decrease in GAXs (Zheng et al., 2023). Similarly, *Phyllostachys edulis*, a monocot, experiences a replacement of mannan/glucomannan with glucuronoarabinoxylans during xylogenesis and a significant increase in the degree of total acetylation substitution (Wang et al., 2019). In contrast, another monocot, sugarcane, retains GAX throughout xylogenesis (Yang et al., 2020). In the dicotyledonous woody flowering plants, *Neolamarckia cadamba* and *Castanopsis hystrix*, GX was detected as the dominant hemicellulose throughout xylogenesis after the stems were lignified (Yang et al., 2022; Zhao et al., 2017). During xylogenesis of cassava, a woody dicotyledonous shrub from the spurge family, XG was gradually replaced with GAX (Yang et al., 2021).

Nelumbo nucifera Gaetn., the sacred lotus, is a perennial aquatic plant with a wide geographical distribution. Classification status of *Nelumbo nucifera Gaetn* exists argument. Once it was classified in the order Nymphaeles due to their structural similarities according to the Cronquist system, but following later molecular phylogenic research, APG (Angiosperm Phylogeny Group) IV, placed it in the order Proteales (Angiosperm Phylogeny Group et al., 2016) in the basal eudicots with mostly terrestrial taxa. Du and Wang (2014) have identified a combination of emergent and floating-leaved life forms of the ancestorial state of *N. nucifera* which is consistent with a terrestrial origin (Du & Wang, 2014). To adapt to an aquatic environment, *N. nucifera* lost vascular cambium during evolution, like the Nymphaeles and the monocots. While the genomes of *N. nucifera* showed no obvious modifications of known key vascular cambium regulators (Povilus et al., 2020). Considering the convergent evolution for aquatic adaptation, it is possible that the hemicelluloses in *N. nucifera* may show greater similarities to aquatic monocots. On the other hand, evolutionary conservatism predicts the hemicellulose from *N. nucifera* is similar with eudicots such as *A. thaliana* and aspen (Bromley et al., 2013; Derba-Maceluch et al., 2015). So it is important to clarify this dispute.

Traditionally, sacred lotus is widely cultivated in China across different climatic zones for various purposes. Recently, there has been a trend of replacing rice fields with lotus plantation ponds in some local government campaigns to boost the income of farmers. However, the petiole, like other agricultural straws, is largely ignored with respect to its potential for increasing the overall added value of the crop. In this study, samples were collected from the apical, middle, and basal segments of the lotus petiole and the hemicellulose was extracted from those segments. By examining the sugar moieties and the spectroscopic characterization of the hemicellulose extracted from each segment, we shed light on the dynamic changes of the hemicellulose during *N. nucifera* xylogenesis. Furthermore, the results were explained in terms of gene expression changes during xylogenesis by transcriptomic analysis. Our research provides new insights into the evolution of angiosperms and provides a valuable foundation for the utilization of this otherwise wasted biomass.

2. Materials and methods

2.1. Materials

Petioles of *N. nucifera* were collected from the South China Botanical Garden in Guangzhou, China. These petioles were subsequently sectioned into three distinct segments: apical, middle, and basal segments as shown in Fig. S1. Each segment measures approximately 7–10 cm and is distinctly separated from the others spatially.

2.2. Hemicellulose extraction

Fresh petiole tissue of lotus was initially rinsed with tap water and subsequently dehydrated in an oven set at 50 °C for three days. The dehydrated material was finely ground to a powder, then treated as previous studies (Wang et al., 2019; Yang et al., 2021). Subsequently, pectin was extracted using digestion in 1 % (*w/v*) calcium oxalate at 80 °C for 4 h. Samples then underwent amylase (α-Amylase from *Bacilus subtilis*) digestion to remove starch following the manufacturer's instructions (Yuanye Bio-Technology, S10002). Finally, hemicelluloses were then produced by alkaline extraction or dimethyl sulfoxide (DMSO)-based extraction as described in a previously published report (Wang et al., 2019; Zheng et al., 2023).

2.3. Microscopic analysis

The sample preparation is mainly derived from Qin et al. (2022). The

petiole segments were first cut into 40-μm sections using a vibrating microtome (Leica Microsystems, Germany). For toluidine blue staining, the sections were incubated with a 0.01 % toluidine blue O solution. These sections were then observed using a bright-field microscope (PreciPoint M8 Imaging System, Germany). The sections were also examined using a xylan-specific antibody, LM10 (Plantprobes, UK), to visualize the distribution of xylan. Briefly, the sections were incubated with the xylan-specific antibody LM10 diluted 20-fold for 1 h at room temperature, followed by incubation with the fluorescein isothiocyanate (FITC) secondary antibody (Zommanbio, China, Cat. ZI319). Samples were mounted on glass slides and observed under a fluorescent microscope (Nikon ECLIPSE Ni—U, Japen).

2.4. Sugar analysis and monosaccharide linkage analysis

Chemical compositions of pretreated crude samples were analyzed according to the standard method of NREL (Sluiter et al., 2008). Briefly, an aliquot (300 mg) of the dry powder of each petiole segment after the removal of starch was first hydrolyzed in 3 mL of 72 % sulfuric acid with agitation at 32 °C for 1 h. After the initial hydrolysis, 84 mL of purified water was added to dilute the acid concentration to 4 %. After drying the crucibles, the weight added to the empty crucibles was measured, representing the acid-insoluble residue. The filtrate was diluted 50-fold using deionized water and analyzed using ion chromatograph equipment (Metrohm 940, Switzerland) equipped with a Dionex™ Carbopac™ PA-20 high-performance anion-exchange chromatography (HPAEC) column. Glucose (Glc), xylose (Xyl), and glucuronic acid (GlcA) concentrations were determined through established standard curves.

For the alkali-extracted hemicellulose, 6 mg of sample was mixed with 0.125 mL of sulfuric acid and 1.35 mL of deionized water referenced by Kuang et al. (2016). The amount of hemicellulosic monosaccharides was determined by fitting the measurement to pre-established standard curves of fucose (Fuc), Glc, Man, Xyl, Gal, Ara, rhamnose (Rha), GlcA and galacturonic acid (GalA).

Monosaccharide linkage analysis for overall cell wall preparations was conducted according to a previously described protocol (Pettolino et al., 2012). Briefly, the plant cell wall sample was prepared using the rapid alcohol-insoluble residue (AIR) method, carboxyl reduced, and then methylated. Derivatives were identified by a combination of retention times and mass spectra. Mol% of each sugar derivative was calculated using standard partially methylated alditol acetates (PMAAs). In each case, two technical replicates of each of two biological replicates were examined. Polysaccharide composition was estimated from monosaccharide linkage composition as described in Pettolino et al. (2012) and further informed by the NMR studies of the hemicellulose fraction.

2.5. Molecular weight determination

The weight average molecular weight (Mw) and number average molecular weight (Mn) were determined following a previously established protocol with minor adjustments (Zhang, Li, Kazachenko, & Xiang, 2023). Initially, The $NaNO_3$-Na_2HPO_4 solution (0.1 M:0.001 M) was used as mobile phase with flow rate 0.6 mL/min. 2 mg of sample from each preparation was dissolved in 1.5 mL of the mobile phase. Subsequently, 10 μL was introduced into the high-performance liquid chromatography apparatus (HPLC) (1260 Infinity, Agilent Technologies, USA) equipped with GPC (gel permeation chromatography) columns (Polymer Laboratories (PL) aquagel-OH 60 and Polymer Laboratories (PL) aquagel-OH MIXED-H, Agilent Technologies, USA). The standard curve was made by dextran with accurate peak molecular weight (Mp:180, 2700, 5250, 9750, 13,050, 36,800, 64,650). The data presented in this study represent the average of two replicates.

2.6. Fourier-transform infrared spectroscopy (FT-IR) analysis

The FT-IR analysis commenced with the preparation of a scanning disk, created by compacting a mixture of 1 mg of either crude petiole sample or alkaline-extracted hemicellulose with 100 mg of KBr. Prior to compression, the mixture underwent thorough grinding and was maintained in a dry state throughout the process. Subsequently, the disk was inserted into the FT-IR spectrophotometer (Vertex 70, Bruker, Germany) and subjected to 32 scans within the range of 2000–500 cm^{-1} with a resolution of 4 cm^{-1} as Zheng et al. (2023).

2.7. Nuclear magnetic resonance (NMR) spectroscopy

All NMR spectroscopy measurements were conducted using a Bruker AV600 spectrometer (Bruker, Germany). The preparation of the samples involved dissolving either 15 or 60 mg of alkaline-extracted hemicellulose in 500 μL deuterium oxide (D_2O) with the addition of a few drops of NaOD, followed by loading into NMR tubes. The ^1H NMR spectrum was measured at 600 MHz. The ^{13}C NMR spectrum underwent 30,000 scans at 25 °C employing a 60° pulse flip angle, a 2-second relaxation time, and a pulse width of 10 μs. The frequency of the ^{13}C spectrum was 74.5 MHz. The HSQC spectrum was obtained in the HSQCGE experimental mode, following previously described parameters (Wang et al., 2019). Data were analyzed using MestReNova.

2.8. Analysis of the degree of acetylation of hemicellulose

Initially, DMSO-extracted hemicellulose underwent hydrolysis using endo-1,4-β-xylanase M1 (Megazyme, Ireland) for 24 h at 50 °C in a 100 mM sodium acetate medium at pH 4.5. Subsequently, the resulting hydrolysate underwent centrifugation (100,000*g*, 1 h), and the supernatant was lyophilized to obtain a xylo-oligosaccharide powder. For NMR analysis, 15 mg of xylo-oligosaccharide was dissolved in 500 μL D_2O and scanned at 600 MHz. The degree of substitution of acetyl groups (DSAC) on the side chains of hemicellulose was calculated using the following equation (Wang et al., 2019):

$$DS_{AC} = \frac{\text{Sum of intergrals for acetyl groups at } 1.9 - 2.0 \text{ ppm}/3}{\text{Sum of intergrals for carbohydrate signals at } 3.0 - 5.5 \text{ ppm}/6}$$

2.9. Reducing end analysis

After starch removal, the samples were dissolved in a solution containing 1 % NaBH4 and 1 M NaOH at a ratio of 1:20 (g to mL). This mixture was incubated overnight at room temperature with vigorous agitation. The resulting solution underwent filtration using a G2 funnel, followed by neutralization using acetic acid. Hemicellulose was obtained following dialysis of the filtrate and subsequent lyophilization. The hemicellulose underwent hydrolysis by a methodology similar to that used in the acetylation substitution analysis (Section 2.8). For ^1H NMR scanning at 600 MHz, 15 mg of the resulting oligosaccharide was used.

2.10. Thermal stability analysis

The hemicellulose extracted using KOH solution was subjected to thermogravimetric analysis using a thermal analyzer from the Waters (USA) (Discovery™ series TGA 550). For each experiment group, 3 mg of sample was used with a heating regime of 10 °C/min from 30 to 700 °C under a constant supply of nitrogen at a rate of 20 mL/min (Zheng et al., 2023).

2.11. Transcriptomic analysis

The “lotus fiber” is the fiber produced by rapturing the petiole and pull (Fig. S2A). Immediately after harvesting from the field, the exterior

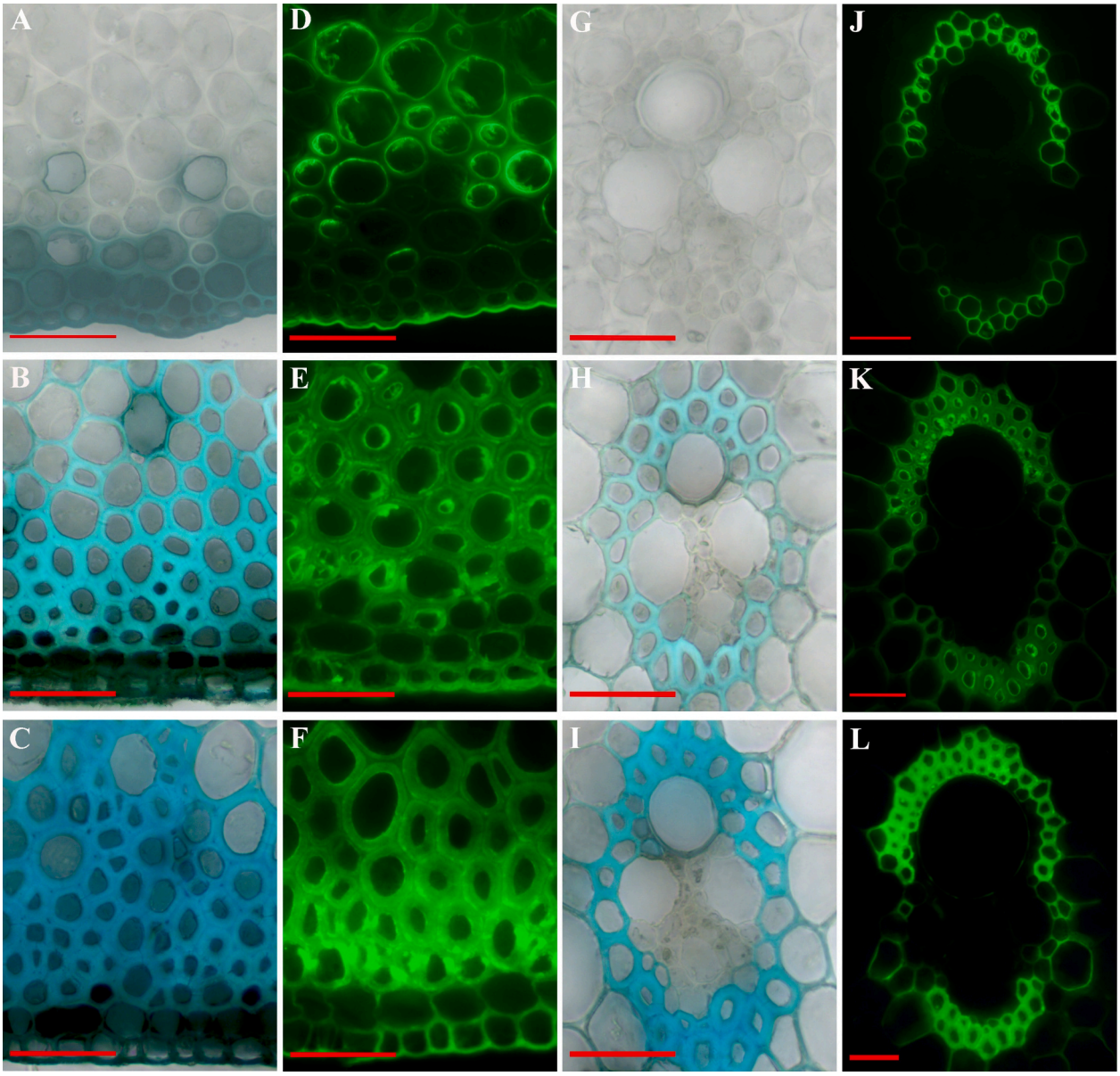

Fig. 1. Cross-sectional microscopic views of the apical, middle and basal segments of the *N. nucifera* petiole. (A–C) The edge stained by toluidine blue O. (D–F) The edge visualized by the LM10 antibody. (G–I) The vascular bundle stained by toluidine blue O. (J–L) The vascular bundle visualized by the LM10 antibody. Apical: A, B, G, J; Middle: B, E, H, K; Basal: C, F, I, L. Bar = 50 μm in all images.

of the petiole is timely peeled by knife. A visualization of the exterior and the interior is shown in Fig. S2A. Each petiole segment from both the exterior and interior were snap-frozen in liquid nitrogen.

The exterior part of the petiole and the "lotus fiber" were used for RNA-seq. The RNA-seq preparation and workflow is mainly derived from Qin et al., 2020. The RNA sequencing (RNA-Seq) process was carried out by Biomarker Technologies Corporation (Beijing, China). High-throughput sequencing was conducted on the NovaSeq 6000 sequencing platform (Illumina, USA), employing a paired-end read length of 150 bp. Bioinformatic analysis was carried out using the BMKcloud online platform (www.biocloud.net) and TBtools (Chen et al., 2020). The sequencing results have been deposited at http://bigd.big.ac.cn/gsa/ under the submission number: CRA013372.

2.12. Statistical analysis

Student *t*-test was conducted using JMP®, Version <18.0.1>. SAS Institute Inc., Cary, NC, 1989–2023. Alpha is set at 0.05.

3. Results and discussion

3.1. Microscopic imaging of the xylogenesis in N. nucifera petiole

Xylogenesis, a temporal developmental process of the vasculature, can be approximately represented and characterized spatially by examining segments of the stem from the apical to the basal regions, representing the nascent/immature to the mature phases, respectively, of xylogenesis. Firstly, microscopic observation was conducted to visualize xylogenesis as it is a fast and convenient method to reveal the morphology and the composition of the cell wall. From the cross-section perspective, the *N. nucifera* petiole is very similar to that of monocots, characterized by scattered vascular bundles and aerenchyma cells (Fig. S2B). The thickness of the cell wall in either the edge area or the vascular bundles increases dramatically from the apical to the basal end as shown by the toluidine blue O staining (Fig. 1A–C, G–I). This thickening is largely caused by an increase in the secondary growth of the fiber cell wall. Furthermore, the increasing darkening of the stain may

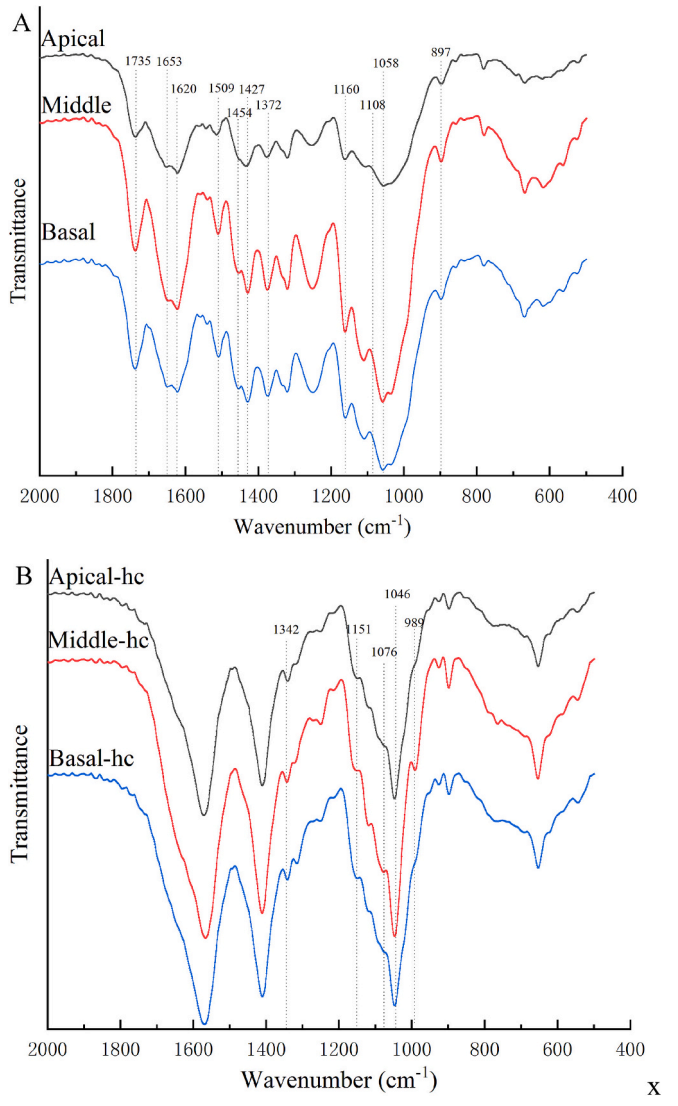

Fig. 2. FT-IR spectra of lotus petiole. A. original samples from the apical, middle, and basal segments. B. hemicellulose fractions extracted from the apical, middle, and basal segments by KOH.

indicate an increased density of acidic hemicellulose, the main components of the SCW. To understand the distribution of xylan in xylogenesis, the xylan-specific LM10 antibody (McCartney et al., 2005) was utilized to visualize xylan in the petiole cross-section by FITC-labelled secondary antibody (Fig. 1D–F, J–L). A relatively weak signal is observed in the apical segment compared with the middle and basal segments. Furthermore, the intensity of the basal segment is only slightly stronger than in the middle. In conclusion, the density of xylan gradually increases during xylogenesis as the SCW continues to be deposited. Our observation of increasing xylan density is in agreement with the findings of an earlier study using LM10 immunolocalization on hybrid aspen xylem tissue (Kim & Daniel, 2012).

Another phenomenon is the patchiness of the fluorescence signal, where the signal is strongly localized in the innermost circle of the cell wall in the apical and middle segments and heavily accumulated near the cell corner and the outmost layer of the cell in the basal segment. Although patchiness is absent in the LM10 fluorescence detection of the Arabidopsis xylem (Peña et al., 2007), it is possible that, when the SCW is actively being deposited, the newly formed SCW is more sensitive to detection by the LM10 antibody, as seen in the apical and middle segments. Like the results in hybrid aspen (Kim & Daniel, 2012), the basal segments of *N. nucifera* petioles show that, in mature fiber cells, more xylan is accumulated in the compound middle lamella. To evaluate the level of interference of lignin auto-fluorescence, negative control samples for each segment was examined using no antibody. For our quasi-quantification resolution, the possible auto-fluorescence signals are neglectable. Overall, the microscopy results suggest the continuous deposition of the SCW both in the vascular bundles and the edge area which is also marked by an increased accumulation of xylan, especially toward the compound middle lamella.

3.2. FT-IR analysis of the N. nucifera petiole

FTIR is a convenient and routinely used analytical technique to examine the chemical characteristics of polymers in plant biomass. To focus on the chemical features of lotus hemicellulose, the original sample and the alkali-extracted hemicellulose sample from each petiole segment were scanned from 2000 to 400 cm^{-1} in a FT-IR spectrometer (Fig. 2). The hemicellulose in the lotus petiole is found to be modified with acetyl groups, as shown by the peak at 1735 cm^{-1} (Fig. 2A) (Pereira et al., 2016). However, acetyl groups are removed in the hemicellulose extraction process using alkali (Fig. 2B). Interestingly, a trend of increasing lignification during xylogenesis is observed, as shown from the increasing intensity of the signal common to all lignin which are the peaks for aromatic skeleton vibration at 1620, 1509 and 1427 cm^{-1}, and C—H deformation at 1454 cm^{-1} (Fig. 2A) (Boeriu et al., 2004). The information about hemicellulose structure is mainly represented in the 1200–1000 cm^{-1} region of the spectrum, although only limited information about the hemicellulose can be mined from the original samples because the hemicellulose signal is masked by overlapping signals from cellulose and lignin.

The data from hemicellulose KOH-extraction in Fig. 2B provide more detailed information. The peak at 1046 cm^{-1} is characteristic of the C-O-C stretching of glycosidic linkages of xylan, suggesting a dominant proportion of xylan in the hemicellulose fraction. Signals for Ara side chains, the shoulder peak at 1151 cm^{-1}, are relatively weak. The anti-symmetric and symmetric stretching vibrations of GlcA groups are represented at 1586 and 1418 cm^{-1}, respectively. In summary, the overall conclusion from our FT-IR scanning study is that the main type of hemicellulose in the lotus petiole is probably a GX with acetyl group modification.

Various methods for hemicellulose isolation had been applied for different research purposes, such as alkali-extraction (Rabetafika et al., 2014), DMSO-extraction (Hägglund et al., 1956) and hot-water extraction (Goldmann et al., 2017). KOH extraction of hemicellulose was selected by us for spectroscopic characterization and chemical composition due to its robustness, high yield and purity (Table S2) (Lawther et al., 1996). However, the acetyl groups attached to the xylan backbone are prone to partly be detached using alkaline solution. DMSO was found to be a milder solvent that retains the acetyl side chains rendering better structural characterization (Naran et al., 2009). Recently, introducing cellulase as a facilitator to the alkali-extraction of hemicellulose (Ding et al., 2019; Hakala et al., 2013; Li et al., 2018) has gained much attention. This strategy was applied to switchgrass hemicellulose extraction demonstrating its effectiveness in maintaining the integrity of the side-chains including methoxyl groups, acetyl groups and 4-*O*-methyl-glucuronic acid (Ding et al., 2019). It is worth considering applying it to the lotus polysaccharide research in the future.

3.3. NMR analysis

NMR is a powerful analytical tool for the resolution of the detailed structure of natural polymers when signal assignments have been assigned from known structures. To better elucidate the hemicellulose structure in the lotus petiole, alkali-extracted hemicellulose from the basal segment was subjected to NMR analysis. The assignment of signature peaks to corresponding atoms was conducted according to the methodologies described in previous studies about hemicellulose (Bian

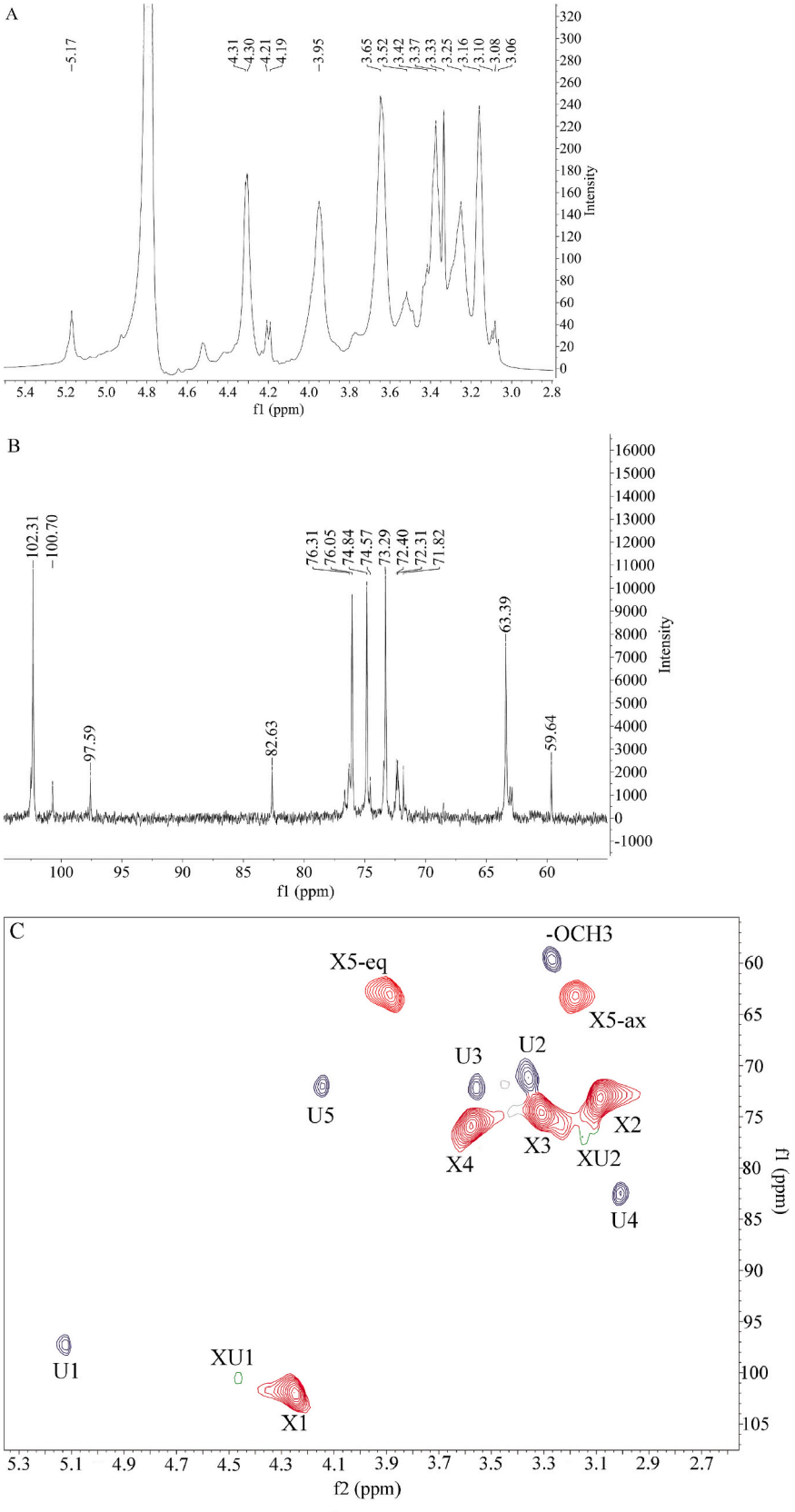

Fig. 3. Hemicellulose structure analysis by NMR. A. ^{1}H NMR spectra of hemicellulose fractions extracted from the basal petiole segment by KOH. B. ^{13}C NMR spectra of hemicellulose fractions extracted from the basal petiole segment. C. HSQC spectra of hemicellulose fractions extracted from the basal petiole segment. X: (1 → 4)-linked β-D-Xyl*p*; U: 4-*O*-methyl-α-D-glucuronic acids; XU: (1 → 4)-β-D-Xyl*p*-2-*O*-(4-OMe-α-D- Glc*p*A); ax = axial, eq = equatorial.

Table 1
The percentage (%) of cellulose, hemicellulose, and Acid Insoluble Residue (AIR) in the petiole of *Nelumbo nucifera*.

	Apical	Middle	Basal
Cellulose	47.76 ± 1.36	55.29 ± 0.76*	56.14 ± 0.74
Hemicellulose	14.31 ± 0.50	16.46 ± 0.53*	16.21 ± 0.41
AIR	37.93 ± 1.67	28.25 ± 1.19*	27.37 ± 1.23

Data are expressed as means ± standard deviations ($n = 4$). Relative percentage is the percentage of a component in the total mass of cellulose, hemicellulose and AIR. AIR is abbreviated for Acid Insoluble Residue.
* indicates the statistical reliability of difference between the * marked group and the previous group based on student *t*-test ($P < 0.05$).

et al., 2012; Peng, Peng, Bian, Xu, & Sun, 2011; Yang et al., 2022; Zhao et al., 2017). The ^{1}H spectrum is shown in Fig. 3A. Unsubstituted (1 → 4)-β-D-Xylp residues can be clearly identified from the spectrum as shown in the major signal at δ 4.31(H1), 3.95(H5-eq), 3.65(H4), 3.37 (H3), 3.25(H5-ax), and 3.16(H2) ppm. In addition, signals originated from 4-*O*-methyl-α-D-Glc*p*A (1 → 2) residues are detected at δ 4.21(H5), 3.52(H2), and 3.33(-OCH_3).

The ^{13}C NMR spectrum confirms the presence of both the non-substituted backbone of D-Xylp and the 4-*O*-methyl-α-D-GlcpA residues, respectively, indicated from the major signals at δ 102.31(C1), 76.05(C4), 74.84(C3), 73.29(C2), and 63.39(C5-ax) ppm for the backbone, and δ 176.99(COOH), 97.59(C1), 82.63(C4), 72.40(C3), 72.31 (C5), 71.82(C2), 59.64(-OCH_3) ppm for the 4-*O*-methyl-α-D-GlcpA. The D-Xylp unit substituted with GlcpA at the O2 position is detected at δ 100.70(C1), 76.31(C2), 74.57(C3) ppm, which are weaker in intensity. It is worth noting that no signal for Araf unit is identified in the ^{13}C NMR spectrum.

To obtain greater resolution of the signals and discover additional information, 2-D HSQC NMR analysis was conducted (Fig. 3C). The ^{13}C/^{1}H cross peaks at δ 102.00/4.25 (X1), 73.18/3.08 (X2), 74.57/3.30 (X3), 76.02/3.57 (X4), 63.26/3.18 (X5-ax), and 63.13/3.88 (X5-eq) are assigned to (1 → 4)-β-D-Xyl*p*, which forms the xylan backbone. The intensity of the non-substituted Xylp unit is relatively strong. Although weaker, the signals for the 4-*O*-methyl-α-D-GlcpA are clearly identified at the cross peaks of δ 97.29/5.12(U1), 71.22/3,35(U2), 72.25/3.55 (U3), 82.53/3.01(U4), 72.15/4.14(U5), and 59.78/3.26(-OCH_3).

Furthermore, the molar ratio of D-Xylp and MeGlcpA residues is calculated to be 14.25: 1, using the corresponding integration of the anomeric region from the HSQC spectra, which falls within the range of typical hardwoods (Ebringerová et al., 2005). The Xylp unit substituted with 4-O-MeGlcpA at the O-2 position has the weakest signals, leaving only the δ 100.64/4.46(C1-H1) and 76.86/3.14(C2-H2) identified. The conclusion reached from our NMR analysis is that the dominant type of hemicellulose in the *N. nucifera* petiole is 4-*O*-methyl-D- glucurono-D-xylan (MGX), with O-2 as the position for 4-O-MeGlcpA.

3.4. Sugar analysis

The mass percentage of the structural polysaccharides, such as cellulose and hemicellulose in the petiole biomass were determined using the NREL protocol (Sluiter et al., 2008) to reveal the dynamic change of biomass composition during xylogenesis. Compared with the apical segment, the relative percentage of cellulose and hemicellulose contents in the middle and basal segments are moderately higher (Table 1) but the ratio between cellulose and hemicellulose are similar, reflecting a constant density of the cell wall matrix. However, the apical segment shows a significant smaller amount of cellulose and hemicellulose in the dry biomass indicating a continuous process of SCW deposition. Lignification is observed to gradually increase from the apical to the basal segments using Wiesner staining (data not shown), a finding which is not reflected in the AIR value.

Hemicellulose monosaccharide composition was determined using HPAEC (Table 2). An increasing trend of relative Xyl concentration and a decreasing trend of Glc concentration are observed which is in congruence with cassava hemicellulose (Yang et al., 2021). This pattern is most possibly due to a gradual deposition of the SCW, leading to more xylan synthesis, while the concentration of XG stops increasing coincident with less primary cell wall (PCW). For xylose content, the difference between the basal and the middle segments is approximately 6 %, whereas the difference between the middle and the apical is about 15 %. This indicates a higher similarity between the middle and the basal segments. The amount of Ara detected for all segments is relatively insignificant as it is of a similar level as that of Fuc, a relatively minor component. This confirmed the HSQC result, in which no Araf side-chain signal was detected in the basal segment hemicellulose. Gal and GlcA, especially in the apical segment, are present at a moderate concentration, which most possibly originate from the pectin extracted alongside the hemicellulose. Thus, the dynamic change of GlcA as a xylan side chain is not reflected from our data.

Table 2
Monosaccharide composition of hemicelluloses extracted by alkali solution from the apical, middle and basal segments of the petiole of *Nelumbo nucifera*.

Monosaccharide	Apical (mg%)	Middle (mg%)	Basal (mg%)
Fuc (fucose)	3.03 ± 0.08	2.54 ± 0.59	1.90 ± 0.53
Rha (rhamnose)	4.88 ± 0.13	5.41 ± 0.80	4.88 ± 0.81
Ara (arabinose)	2.78 ± 0.12	3.00 ± 0.46	2.80 ± 0.58
Gal (galactose)	10.37 ± 0.16	7.90 ± 0.86*	6.48 ± 0.80*
Glc (glucose)	18.03 ± 0.32	8.01 ± 1.07*	4.82 ± 0.42*
Xyl (xylose)	50.97 ± 0.48	65.61 ± 2.20*	71.23 ± 1.19*
GalA (galacturonic acid)	3.22 ± 0.17	3.69 ± 1.31	3.71 ± 1.62
GlcA (glucuronic acid)	6.72 ± 0.35	3.84 ± 1.34*	4.19 ± 0.60

Data are presented as means ± standard deviation (n = 4).
* indicates the statistical reliability of difference between the * marked group and the previous group based on student *t*-test ($P < 0.05$).

Table 3
Polysaccharide composition (mol %) of the exterior division, interior division of the middle segment of lotus petiole, and lotus fibers.

	Exterior petiole	Internal petiole	Lotus fibers
Pectic polysaccharides			
Arabinan	2.73	1.96	1.44
Type I AG	5.90	6.14	3.99
Type II AG	2.12	5.10	1.52
Homogalacturonan	2.53	3.09	0.16
RG I	1.09	1.59	0.25
Glucuronoxylan	26.29	15.59	28.26
Heteromannan	6.17	7.24	3.69
Xyloglucan	7.82	7.45	3.52
Callose	0.37	0.79	1.12
Extensin	0.38	0.63	0.16
Total	93.75	94.89	96.03

To better understand the composition of the cell wall of the lotus petiole, linkage analysis using methylation (Pettolino et al., 2012) was used on the exterior and interior components of the middle segment of the lotus petiole, and on lotus fibers which are produced from the rupture of the petiole, possibly representing the thickened secondary wall of vascular bundles (Table 3; for complete table, see Table S3) (Pan et al., 2011). The proportion of heteroxylan to cellulose in the exterior component is three times that of the interior component. The amount of 1,3-Ara-f is negligible, a finding which is consistent with the HSQC data. Little Man was detected, which is in agreement with the findings from HPAEC-based analysis.

3.5. Molecular weight

The size (molecular weight (MW)) of the xylan molecule is important in the quality control aspects of various industries which use xylan as it impacts the solubility and viscosity of xylan and its interaction with

Table 4
Molecular weight of the hemicellulose extracted by alkaline from the apical, middle and basal segments of the lotus petiole.

	Mw	Mn	Mw/Mn
Apical	108,349	76,257	1.42
Middle	117,233	96,620	1.21
Basal	112,390	93,412	1.20

Data are presented as means ($n = 2$).

other molecules. Moreover, the interaction between xylan and both cellulose and lignin are influenced by the xylan MW (Kabel et al., 2007; Westbye et al., 2007). To better characterize the dynamic changes in hemicellulose during xylogenesis in *N. nucifera*, the MW of the hemicellulose extracted from the apical, middle, and basal segments of the petiole was determined using HPLC. The difference in MW of the hemicellulose between that extracted from the middle and the basal segments is moderate (Table 4; see the distribution curves in Fig. S3). In contrast, the hemicellulose MW from the apical segment is much lower. And the Mw/Mn ratio is much greater than that from the other two segments, suggesting a lower homogeneity of the apical hemicellulose. The MW profile of the apical hemicellulose may be due to more diverse hemicellulose species, active synthesis processes, and lower purity.

3.6. Reducing end

A unique tetrasaccharide sequence, β-Xyl-(1,3)-α-Rha-(1,2)-α-GalA-(1,4)-Xyl, is present at the reducing end of xylan from gymnosperms, dicots, and some monocots (Ye & Zhong, 2022). The sequence is likely a primer for the initiation of xylan backbone synthesis. To verify the presence of the tetrasaccharide in *N. nucifera*, the ^{1}H NMR spectrum was acquired, using oligosaccharides from the digestion of alkali-extracted hemicellulose from the basal segment of the petiole (Fig. 4). Compared with the corresponding spectrum from *A. thaliana* (Peña et al., 2007), the lotus spectrum was, as predicted, highly similar and the protons belonging to the GalA (galacturonic acid), Rha (rhamnose) and 3-linked-β-Xylose unit was identified. Combined with our previous results, we concluded that a tetrasaccharide sequence typical of dicots was present in the lotus glucuronoxylan.

3.7. Xylan acetyl substitution

Xylans from angiosperms are acetylated at O-2 and/or O-3 with the degree of acetyl substitution ranging from 20 % to 70 % (Zhong et al., 2017). DMSO was used as the solvent, instead of alkali which would remove the acetyl groups, for the hemicellulose extraction to maximize the integrity of acetyl groups (Hägglund et al., 1956; Zhong et al., 2018), and the subsequent hemicellulose extractions from each segment of the petiole were subjected to ^{1}H NMR scanning to characterize the acetyl substitutions which are represented by the region around 2.10 ppm (Fig. 5). Different type of acetyl substitution can be separately identified from the spectrum where δ 2.18, 2.13, 2.12 and 2.07 ppm correspond to 3-*O*-acetylated (Ac) 2-*O*-GlcA-substituted (Xyl-3Ac-2GlcA),2-*O*-monoacetylated (Xyl-2Ac), 3-*O*-monoacetylated (Xyl-3Ac), and 2, 3-di-*O*-acetylated (Xyl-2,3Ac), respectively (Neumüller et al., 2015). Acetylation during xylogenesis increases to a steady state, as shown by our calculation of the total degree of substitutions by acetyl groups (DSAC), where the apical, middle, and basal segments of the lotus petiole are 0.45, 054, and 0.55, respectively (Table 5).

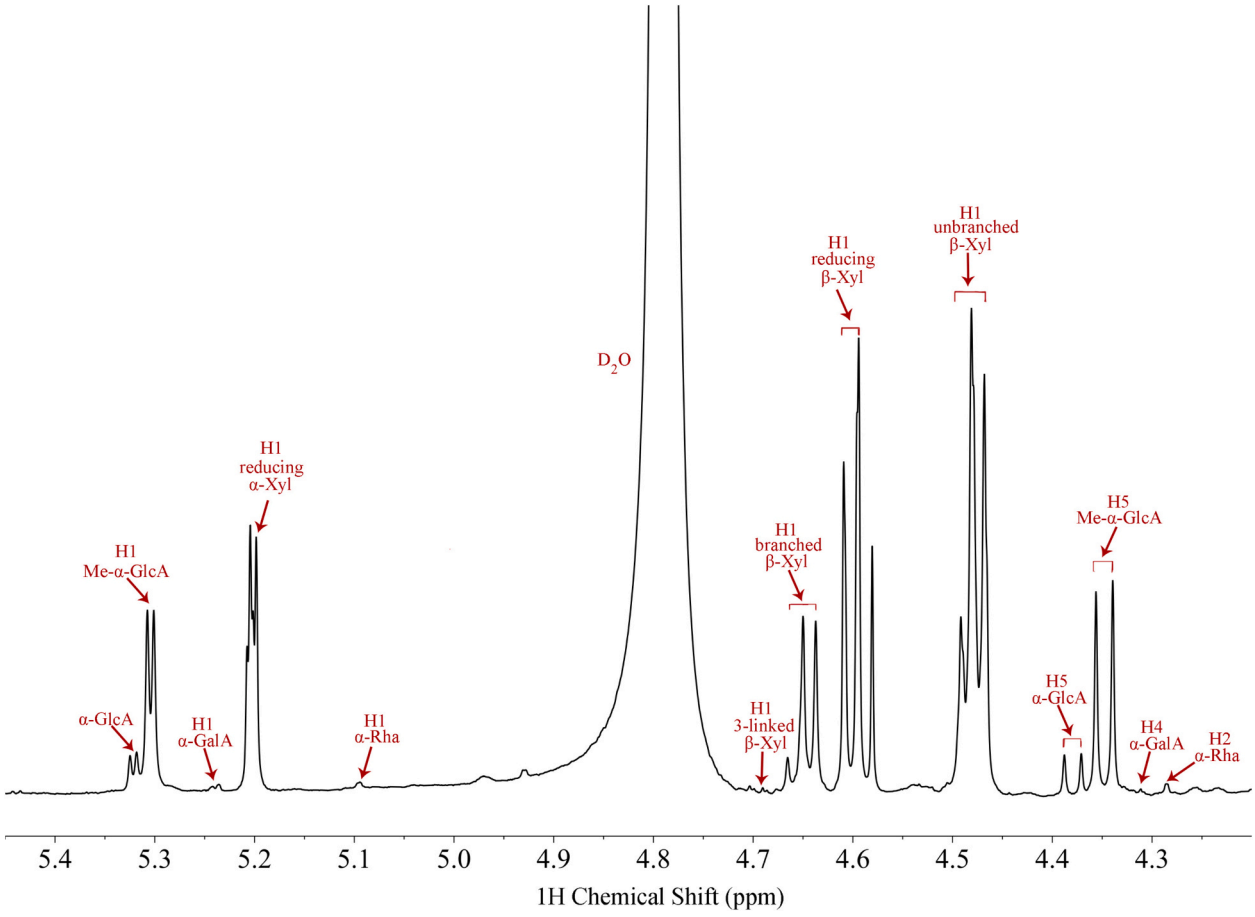

Fig. 4. Anomeric region of the ^{1}H NMR spectra of the xylo-oligosaccharides generated by endoxylanase digestion of the basal segment solubilized by 1 M NaOH (contained 0.1 % NaBH4).

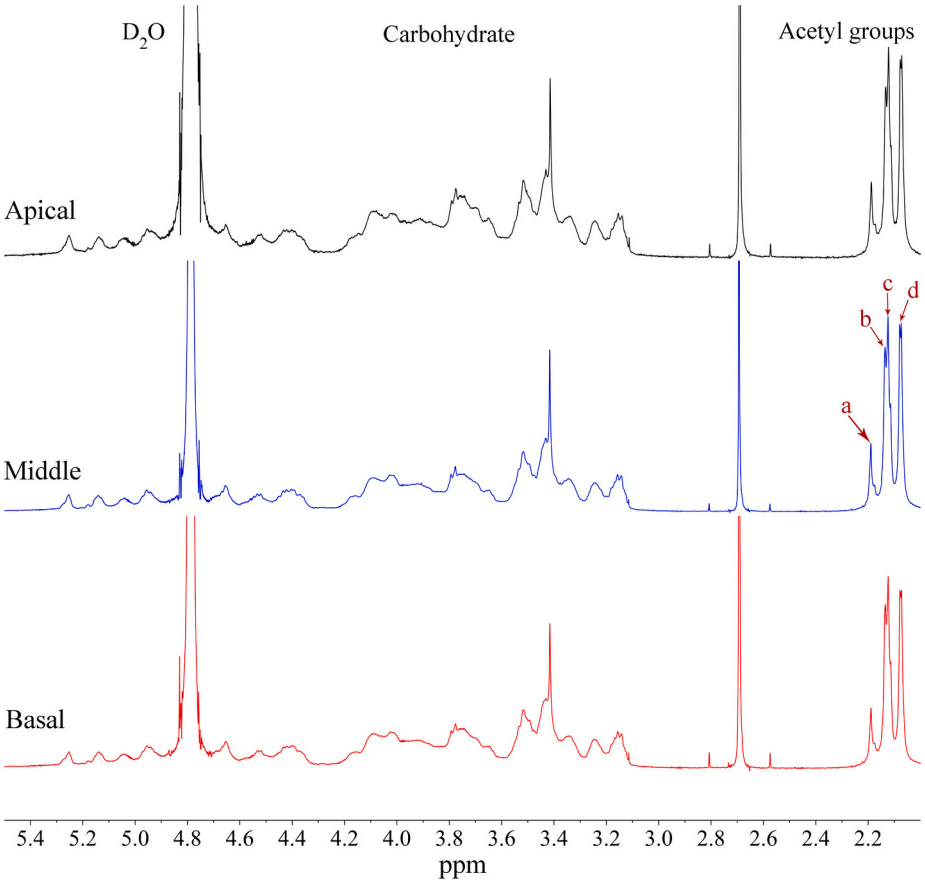

Fig. 5. ^{1}H NMR spectra of acetyl xylooligomers extracted by DMSO and digested by endoxylanase. A: apical B: middle C: basal segments of the petiole. a: Xyl-3Ac-2GlcA; b: Xyl-2Ac; c: Xyl-3Ac; d: Xyl-2,3Ac.

Table 5
The degree of substitution by acetyl groups (DS_{AC}) in lotus hemicellulose from different segments of the petiole.

	Carbohydrate	Acetyl	DS_{AC}
Apical	4.44	1.00	0.45
Middle	3.7	1.00	0.54
Basal	3.62	1.00	0.55

Data are presented as means ($n = 2$).

3.8. Thermogravimetric analysis

The thermal stability of hemicellulose extracted from the lotus petiole using KOH solution was examined using thermogravimetric analysis (TGA). Three stages can be identified from the mass curve (Fig. 6A). The first stage corresponds to the vaporization of water molecules and ranges from the beginning to 170 °C. The second stage, from 170 to 355 °C, corresponds to the decomposition of the hemicellulose. The carbonization stage, the third stage, happened after 550 °C where chars are formed. Our results are like a slightly left-shifted version of the already-published numerical values from poplar and oak, where the decomposition starts at 150 °C and reaches the peak at 220 °C (Jin et al., 2013). Such differences may be caused by variability among xylan source or TGA conditions. From the perspective of derivative thermogravimetric (DTG) analysis, a slower depolymerization rate is observed in the basal hemicellulose whereas the rates in the apical and the middle segments are almost identical in the acceleration phase of the decomposition rate (Fig. 6B). However, the apical hemicellulose enters the decomposition earlier than the other two, indicating a weaker thermal stability. In conclusion, the thermal stability of the hemicellulose extracts gradually increases during xylogenesis. Thermal stability of xylan is proportional to the degree of acetyl modification, crystalline and amorphous regions, molecular weight and linearity of the polymer structures (Carvalho et al., 2019; Peng, Peng, Bian, Xu, Sun, & Kennedy, 2011). So, the higher thermal stability of the basal section may originate in many factors.

3.9. Transcriptomic analysis

To shed light on the underlying gene expression profiles associated with the dynamic changes of hemicellulose during xylogenesis, transcriptomic analysis was conducted on the exterior region of all segments of lotus petiole. Heatmaps of xylan-, xyloglucan-, galactan- and arabinan-synthesis-related genes were generated by TBtools (Chen et al., 2020). For xylan-biosynthesis-related activities, the apical segment shows the lowest activities, while the middle segment shows the highest activities for both the backbone elongation and side chain modification genes (Fig. 7). This trend we observed is not fully consistent with the trend observed in *N. cadamba* (Zhao et al., 2014), where the basal segment has a higher expression level. As shown in Fig. 7, the main biosynthetic activity in the apical segment is xyloglucan biosynthesis, as both the backbone and side chain modification genes of xyloglucan are at the highest levels of expression. A higher level of galactan biosynthesis was also observed in the apical segment, which partly explains the higher proportion of Gal among the minor sugars in the hemicellulose fraction of the apical segment. Taken together, these findings indicate that the apical segment is predominantly occupied with primary cell wall generation.

The compositional and structural differences between the middle and the basal glucuronoxylan (GX) is relatively trivial, as found

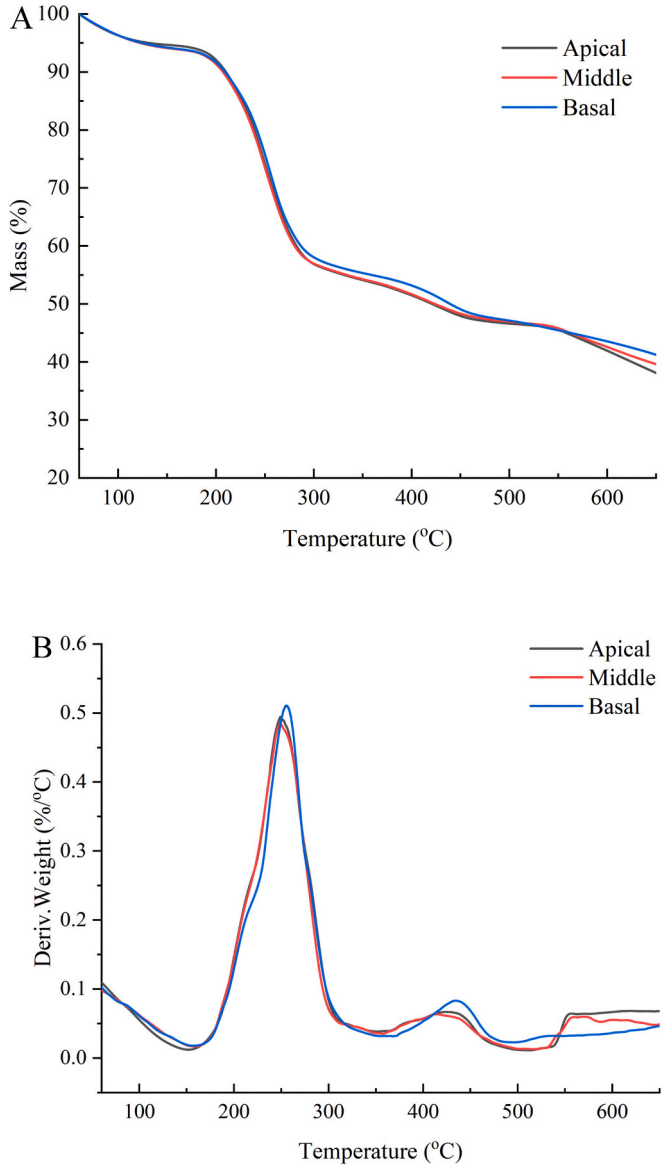

Fig. 6. Thermal gravimetric analysis of the lotus samples. A. Mass curves of hemicellulose extracted from the apical, middle, and basal segments of the lotus petiole. B. The mass loss rate curves of hemicellulose extracted from the apical, middle, and basal segments of the lotus petiole.

previously (Yang et al., 2022). The xylan biosynthesis genes in the basal segment are expressed at a lower level than in the middle segment but the difference is not as significant as that between the apical and the middle. This result may indicate that, when the xylan in the SCW reaches its mature size and fully interacts with the surrounding lignin and cellulose, its biosynthesis will slow down.

4. Conclusion

During the xylogenesis process in *N. nucifera*, the hemicellulose profiles underwent various notable changes in a spatio-temporal sequence of development. The apical segment of the petiole, representing the initial (immature) phase of xylogenesis, is predominantly composed of xyloglucan in terms of hemicellulose composition. Accordingly, xyloglucan biosynthesis in the apical segment is more active than xylan biosynthesis. The dominant hemicellulose switches to glucuronoxylan in the middle and the basal segments. In addition, the presence of a signature tetrasaccharide sequence at the reducing end

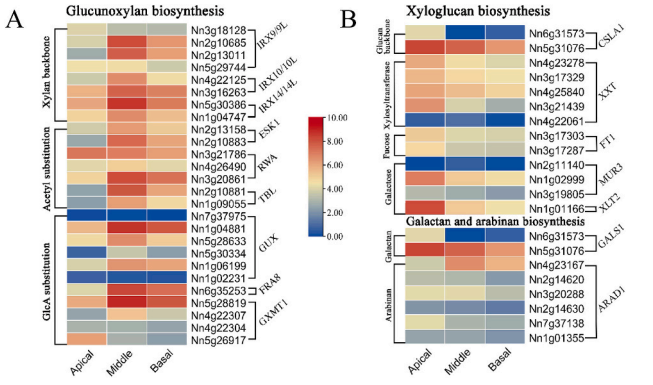

Fig. 7. Heatmap of the expression levels of biosynthesis genes of glucunoxylans (A), xyloglucans (B), and some pectins in different segments of the lotus petiole (B). IRX, irregular xylem; ESK, ESKIMO. RWA, reduced wall acetylation; TBL, trichome birefringence-like; GUX, glucuronic acid substitution of xylan; GATL, galacturonosyl transferase-like; GUX, glucuronic acid substitution of xylan; RWA, reduced wall acetylation; TBL, trichome birefringence-like; ESK, ESKIMO. FRA, fragile fiber; GXMT, glucuronoxylan methyltransferase; CSLA cellulose synthase like-A; XXT, xyloglucan xylosyltransferase; FT, fucosyltransferase; MUR, MURUS; XLT, xyloglucan L-side chain galactosyltransferase; GALS, galactan synthase; ARAD, arabinan deficient.

was confirmed by NMR spectroscopy. In terms of the side chains of the lotus xylan, multiple lines of evidence demonstrated that the 4-O-GlcA and acetyl substitutions are the only types of modification. The degree of acetylation gradually increases from the apical to the basal segment. The difference between the middle and the basal is not as significant as the difference from either to the apical segment. However, the synthesis of xylan is more active in the middle segment, as demonstrated by the related gene expression heatmap and the distribution of xylan *in mura*. Our characterization of lotus hemicellulose is the first in this basal eudicot to the best of our knowledge and the results indicate that hemicellulose is highly conserved in dicotyledonous plants.

CRediT authorship contribution statement

Anran Feng: Conceptualization, Data curation, Methodology, Writing – original draft, Writing – review & editing. **Yingying Guan:** Conceptualization, Methodology, Validation. **Haoqiang Yang:** Methodology, Validation. **Biao Zheng:** Methodology, Validation, Visualization. **Wei Zeng:** Methodology. **Pengfei Hao:** Methodology. **Antony Bacic:** Writing – review & editing. **Shi-you Ding:** Conceptualization, Supervision, Writing – review & editing. **Ai-min Wu:** Conceptualization, Funding acquisition, Investigation, Supervision, Writing – review & editing.

Declaration of competing interest

The authors declare that they have no known competing financial interests or personal relationships that could have appeared to influence the work reported in this paper.

Acknowledgement

Firstly, we would like to thank for the generosity of South China Botanical Garden that allowed us to collect the samples used in our study. During the harvest of material, Zi-jian Mou and Zi-cai Xie, graduate students from the South China Botanical Garden, offered us a great deal of assistance and convenience which are vastly appreciated. AB, WZ and PH acknowledge the support of La Trobe University to LISAF. Anran Feng is supported by U.S. Department of Energy, Office of Science, Biological and Environmental Research Program, under Award Number DE-SC0019072.

Appendix A. Supplementary data

Supplementary data to this article can be found online at https://doi.org/10.1016/j.carbpol.2024.122940.

Data availability

Data will be made available on request.

References

Angiosperm Phylogeny Group, Chase, M. W., Christenhusz, M. J., Fay, M. F., Byng, J. W., Judd, W. S., et al. (2016). An update of the Angiosperm Phylogeny Group classification for the orders and families of flowering plants: APG IV. *Botanical Journal of the Linnean Society, 181*(1), 1–20.

Bian, J., Peng, F., Peng, P., Xu, F., & Sun, R. C. (2012). Chemical composition and structural feature of Populus gansuensis hemicellulosic polymers. *Journal of Applied Polymer Science, 124*(4), 3154–3164.

Boeriu, C. G., Bravo, D., Gosselink, R. J., & van Dam, J. E. (2004). Characterisation of structure-dependent functional properties of lignin with infrared spectroscopy. *Industrial Crops and Products, 20*(2), 205–218.

Bromley, J. R., Busse-Wicher, M., Tryfona, T., Mortimer, J. C., Zhang, Z., Brown, D. M., & Dupree, P. (2013). GUX 1 and GUX 2 glucuronyltransferases decorate distinct domains of glucuronoxylan with different substitution patterns. *The Plant Journal, 74*(3), 423–434.

Brown, D. M., Goubet, F., Wong, V. W., Goodacre, R., Stephens, E., Dupree, P., & Turner, S. R. (2007). Comparison of five xylan synthesis mutants reveals new insight into the mechanisms of xylan synthesis. *The Plant Journal, 52*(6), 1154–1168.

Capek, P., Kubačková, M., Alföldi, J., Bilisics, L., Lišková, D., & Kákoniová, D. (2000). Galactoglucomannan from the secondary cell wall of Picea abies L. *Karst. Carbohydrate Research, 329*(3), 635–645.

Carvalho, D. M., Berglund, J., Marchand, C., Lindström, M. E., Vilaplana, F., & Sevastyanova, O. (2019). Improving the thermal stability of different types of xylan by acetylation. *Carbohydrate Polymers, 220*, 132–140.

Chen, C., Chen, H., Zhang, Y., Thomas, H. R., Frank, M. H., He, Y., & Xia, R. (2020). TBtools: An integrative toolkit developed for interactive analyses of big biological data. *Molecular Plant, 13*(8), 1194–1202.

Cocuron, J. C., Lerouxel, O., Drakakaki, G., Alonso, A. P., Liepman, A. H., Keegstra, K., et al. (2007). A gene from the cellulose synthase-like C family encodes a β-1, 4 glucan synthase. *Proceedings of the National Academy of Sciences, 104*(20), 8550–8555.

Darvill, J. E., McNeil, M., Darvill, A. G., & Albersheim, P. (1980). Structure of Plant Cell Walls: XI. Glucuronoarabinoxylan, a second hemicellulose in the primary cell walls of suspension-cultured sycamore cells. *Plant Physiology, 66*(6), 1135–1139.

Derba-Maceluch, M., Awano, T., Takahashi, J., Lucenius, J., Ratke, C., Kontro, I., et al. (2015). Suppression of xylan endotransglycosylase PtxtXyn10A affects cellulose microfibril angle in secondary wall in aspen wood. *New Phytologist, 205*(2), 666–681.

Ding, J., Yoo, C. G., Pu, Y., Meng, X., Bhagia, S., Yu, C., & Ragauskas, A. J. (2019). Cellulolytic enzyme-aided extraction of hemicellulose from switchgrass and its characteristics. *Green Chemistry, 21*(14), 3902–3910.

Du, Z. Y., & Wang, Q. F. (2014). Correlations of life form, pollination mode and sexual system in aquatic angiosperms. *PLoS One, 9*(12), Article e115653.

Ebringerová, A., Hromádková, Z., & Heinze, T. (2005). *Hemicellulose* (pp. 1–67). Polysaccharides I: Structure, characterization and use.

Eseyin, A. E., & Steele, P. H. (2015). *An overview of the applications of furfural and its derivatives*.

Fischer, M. H., Yu, N., Gray, G. R., Ralph, J., Anderson, L., & Marlett, J. A. (2004). The gel-forming polysaccharide of psyllium husk (Plantago ovata Forsk). *Carbohydrate Research, 339*(11), 2009–2017.

Goldmann, W. M., Ahola, J., Mikola, M., & Tanskanen, J. (2017). Formic acid aided hot water extraction of hemicellulose from European silver birch (Betula pendula) sawdust. *Bioresource Technology, 232*, 176–182.

Hägglund, E. R. I. K., Lindberg, B., & McPherson, J. (1956). Dimethylsulphoxide, a solvent for hemicelluloses. *Acta Chemica Scandinavica, 10*, 1160–1164.

Hakala, T. K., Liitiä, T., & Suurnäkki, A. (2013). Enzyme-aided alkaline extraction of oligosaccharides and polymeric xylan from hardwood kraft pulp. *Carbohydrate Polymers, 93*(1), 102–108.

Hansen, N. M., & Plackett, D. (2008). Sustainable films and coatings from hemicelluloses: A review. *Biomacromolecules, 9*(6), 1493–1505.

Jiang, N., Wiemels, R. E., Soya, A., Whitley, R., Held, M., & Faik, A. (2016). Composition, assembly, and trafficking of a wheat xylan synthase complex. *Plant Physiology, 170*(4), 1999–2023.

Jin, W., Singh, K., & Zondlo, J. (2013). Pyrolysis kinetics of physical components of wood and wood-polymers using isoconversion method. *Agriculture, 3*(1), 12–32.

Kabel, M. A., van den Borne, H., Vincken, J. P., Voragen, A. G., & Schols, H. A. (2007). Structural differences of xylans affect their interaction with cellulose. *Carbohydrate Polymers, 69*(1), 94–105.

Kim, J. S., & Daniel, G. (2012). Distribution of glucomannans and xylans in poplar xylem and their changes under tension stress. *Planta, 236*, 35–50.

Kim, S. J., Chandrasekar, B., Rea, A. C., Danhof, L., Zemelis-Durfee, S., Thrower, N., et al. (2020). The synthesis of xyloglucan, an abundant plant cell wall polysaccharide, requires CSLC function. *Proceedings of the National Academy of Sciences, 117*(33), 20316–20324.

Kuang, B., Zhao, X., Zhou, C., Zeng, W., Ren, J., Ebert, B., et al. (2016). Role of UDP-glucuronic acid decarboxylase in xylan biosynthesis in Arabidopsis. *Molecular Plant, 9*(8), 1119–1131.

Lawther, J. M., Sun, R., & Banks, W. B. (1996). Effects of extraction conditions and alkali type on yield and composition of wheat straw hemicellulose. *Journal of Applied Polymer Science, 60*(11), 1827–1837.

Lee, C., Teng, Q., Huang, W., Zhong, R., & Ye, Z. H. (2009). The F8H glycosyltransferase is a functional paralog of FRA8 involved in glucuronoxylan biosynthesis in Arabidopsis. *Plant and Cell Physiology, 50*(4), 812–827.

Lee, C., Teng, Q., Zhong, R., & Ye, Z. H. (2011). Molecular dissection of xylan biosynthesis during wood formation in poplar. *Molecular Plant, 4*(4), 730–747.

Lee, C., Teng, Q., Zhong, R., & Ye, Z. H. (2012). Arabidopsis GUX proteins are glucuronyltransferases responsible for the addition of glucuronic acid side chains onto xylan. *Plant and Cell Physiology, 53*(7), 1204–1216.

Lee, C., Teng, Q., Zhong, R., Yuan, Y., Haghighat, M., & Ye, Z. H. (2012). Three Arabidopsis DUF579 domain-containing GXM proteins are methyltransferases catalyzing 4-O-methylation of glucuronic acid on xylan. *Plant and Cell Physiology, 53*(11), 1934–1949.

Lee, C., Zhong, R., Richardson, E. A., Himmelsbach, D. S., McPhail, B. T., & Ye, Z. H. (2007). The PARVUS gene is expressed in cells undergoing secondary wall thickening and is essential for glucuronoxylan biosynthesis. *Plant and Cell Physiology, 48*(12), 1659–1672.

Li, J., Zhang, S., Li, H., Ouyang, X., Huang, L., Ni, Y., & Chen, L. (2018). Cellulase pretreatment for enhancing cold caustic extraction-based separation of hemicelluloses and cellulose from cellulosic fibers. *Bioresource Technology, 251*, 1–6.

McCartney, L., Marcus, S. E., & Knox, J. P. (2005). Monoclonal antibodies to plant cell wall xylans and arabinoxylans. *Journal of Histochemistry and Cytochemistry, 53*(4), 543–546.

Mortimer, J. C., Miles, G. P., Brown, D. M., Zhang, Z., Segura, M. P., Weimar, T., et al. (2010). Absence of branches from xylan in Arabidopsis gux mutants reveals potential for simplification of lignocellulosic biomass. *Proceedings of the National Academy of Sciences, 107*(40), 17409–17414.

Naran, R., Black, S., Decker, S. R., & Azadi, P. (2009). Extraction and characterization of native heteroxylans from delignified corn stover and aspen. *Cellulose, 16*, 661–675.

Naran, R., Chen, G., & Carpita, N. C. (2008). Novel rhamnogalacturonan I and arabinoxylan polysaccharides of flax seed mucilage. *Plant Physiology, 148*(1), 132–141.

Neumüller, K. G., Souza, A. C.d., Rijn, J. H., Streekstra, H., Gruppen, H., & Schols, H. A. (2015). Positional preferences of acetyl esterases from different CE families towards acetylated 4-O-methyl glucuronic acid-substituted xylo-oligosaccharides. *Biotechnology for Biofuels, 8*(1), 7.

Pan, Y., Han, G., Mao, Z., Zhang, Y., Huang, J., & Qu, L. (2011). The anatomy of lotus fibers found in petioles of Nelumbo nucifera. *Aquatic Botany, 95*(2), 167–171.

Peña, M. J., Zhong, R., Zhou, G. K., Richardson, E. A., O'Neill, M. A., Darvill, A. G., et al. (2007). Arabidopsis irregular xylem8 and irregular xylem9: Implications for the complexity of glucuronoxylan biosynthesis. *The Plant Cell, 19*(2), 549–563.

Peng, P., Peng, F., Bian, J., Xu, F., & Sun, R. (2011). Studies on the starch and hemicelluloses fractionated by graded ethanol precipitation from bamboo Phyllostachys bambusoides f. shouzhu Yi. *Journal of Agricultural and Food Chemistry, 59*(6), 2680–2688.

Peng, P., Peng, F., Bian, J., Xu, F., Sun, R. C., & Kennedy, J. F. (2011). Isolation and structural characterization of hemicelluloses from the bamboo species Phyllostachys incarnata Wen. *Carbohydrate Polymers, 86*(2), 883–890.

Pereira, S. C., Maehara, L., Machado, C. M., & Farinas, C. S. (2016). Physical–chemical–morphological characterization of the whole sugarcane lignocellulosic biomass used for 2G ethanol production by spectroscopy and microscopy techniques. *Renewable Energy, 87*, 607–617.

Pettolino, F. A., Walsh, C., Fincher, G. B., & Bacic, A. (2012). Determining the polysaccharide composition of plant cell walls. *Nature Protocols, 7*(9), 1590–1607.

Popper, Z. A. (2008). Evolution and diversity of green plant cell walls. *Current Opinion in Plant Biology, 11*(3), 286–292.

Povilus, R. A., DaCosta, J. M., Grassa, C., Satyaki, P. R., Moeglein, M., Jaenisch, J., et al. (2020). Water lily (Nymphaea thermarum) genome reveals variable genomic signatures of ancient vascular cambium losses. *Proceedings of the National Academy of Sciences, 117*(15), 8649–8656.

Qin, W., Wang, N., Yin, Q., Li, H., Wu, A. M., & Qin, G. (2022). Activation tagging identifies WRKY14 as a repressor of plant thermomorphogenesis in Arabidopsis. *Molecular Plant, 15*(11), 1725–1743.

Qin, W., Yin, Q., Chen, J., Zhao, X., Yue, F., He, J., et al. (2020). The class II KNOX transcription factors KNAT3 and KNAT7 synergistically regulate monolignol biosynthesis in Arabidopsis. *Journal of Experimental Botany, 71*(18), 5469–5483.

Rabetafika, H. N., Bchir, B., Blecker, C., Paquot, M., & Wathelet, B. (2014). Comparative study of alkaline extraction process of hemicelluloses from pear pomace. *Biomass and Bioenergy, 61*, 254–264.

Scheller, H. V., & Ulvskov, P. (2010). Hemicelluloses. *Annual Review of Plant Biology, 61*, 263–289.

Sista Kameshwar, A. K., & Qin, W. (2018). Understanding the structural and functional properties of carbohydrate esterases with a special focus on hemicellulose deacetylating acetyl xylan esterases. *Mycology, 9*(4), 273–295.

Sluiter, A., Hames, B., Ruiz, R., Scarlata, C., Sluiter, J., Templeton, D., & Crocker, D. L. A. P. (2008). Determination of structural carbohydrates and lignin in biomass. *Laboratory analytical procedure, 1617*(1), 1–16.

Urbanowicz, B. R., Peña, M. J., Ratnaparkhe, S., Avci, U., Backe, J., Steet, H. F., et al. (2012). 4-O-methylation of glucuronic acid in Arabidopsis glucuronoxylan is catalyzed by a domain of unknown function family 579 protein. *Proceedings of the National Academy of Sciences, 109*(35), 14253–14258.

Wang, H., Yang, H., Wen, Z., Gao, C., Gao, Y., Tian, Y., et al. (2022). Xylan-based nanocompartments orchestrate plant vessel wall patterning. *Nature Plants, 8*(3), 295–306.

Wang, K. L., Wang, B., Hu, R., Zhao, X., Li, H., Zhou, G., et al. (2019). Characterization of hemicelluloses in Phyllostachys edulis (moso bamboo) culm during xylogenesis. *Carbohydrate Polymers, 221*, 127–136.

Wang, L., Wu, M., & Liu, H. M. (2017). Emulsifying and physicochemical properties of soy hull hemicelluloses-soy protein isolate conjugates. *Carbohydrate Polymers, 163*, 181–190.

Westbye, P., Köhnke, T., Glasser, W., & Gatenholm, P. (2007). The influence of lignin on the self-assembly behaviour of xylan rich fractions from birch (Betula pendula). *Cellulose, 14*, 603–613.

Wu, A. M., Hörnblad, E., Voxeur, A., Gerber, L., Rihouey, C., Lerouge, P., & Marchant, A. (2010). Analysis of the Arabidopsis IRX9/IRX9-L and IRX14/IRX14-L pairs of glycosyltransferase genes reveals critical contributions to biosynthesis of the hemicellulose glucuronoxylan. *Plant Physiology, 153*(2), 542–554.

Wu, A. M., Rihouey, C., Seveno, M., Hörnblad, E., Singh, S. K., Matsunaga, T., et al. (2009). The Arabidopsis IRX10 and IRX10-LIKE glycosyltransferases are critical for glucuronoxylan biosynthesis during secondary cell wall formation. *The Plant Journal, 57*(4), 718–731.

Xu, Y., Liu, K., Yang, Y., Kim, M. S., Lee, C. H., Zhang, R., et al. (2023). Hemicellulose-based hydrogels for advanced applications. *Frontiers in Bioengineering and Biotechnology, 10*, Article 1110004.

Yang, H., Yi, N., Zhao, S., Qaseem, M. F., Zheng, B., Li, H., et al. (2020). Characterization of hemicelluloses in sugarcane (Saccharum spp. hybrids) culm during xylogenesis. *International Journal of Biological Macromolecules, 165*, 1119–1128.

Yang, H., Yi, N., Zhao, S., Xiang, Z., Qaseem, M. F., Zheng, B., et al. (2021). Characterization of hemicellulose in Cassava (Manihot esculenta Crantz) stem during xylogenesis. *Carbohydrate Polymers, 264*, Article 118038.

Yang, H. Q., Zheng, B., Xiang, Z., Qaseem, M. F., Zhao, S., Li, H., Feng, J. X., et al. (2022). Characterization of hemicellulose during xylogenesis in rare tree species Castanopsis hystrix. *International Journal of Biological Macromolecules, 212*, 348–357.

Ye, Z. H., & Zhong, R. (2022). Outstanding questions on xylan biosynthesis. *Plant Science, 111476*.

Yuan, Y., Teng, Q., Lee, C., Zhong, R., & Ye, Z. H. (2014). Modification of the degree of 4-O-methylation of secondary wall glucuronoxylan. *Plant Science, 219*, 42–50.

Yuan, Y., Teng, Q., Zhong, R., Haghighat, M., Richardson, E. A., & Ye, Z. H. (2016). Mutations of Arabidopsis TBL32 and TBL33 affect xylan acetylation and secondary wall deposition. *PLoS One, 11*(1), Article e0146460.

Zablackis, E., Huang, J., Muller, B., Darvill, A. G., & Albersheim, P. (1995). Characterization of the cell-wall polysaccharides of Arabidopsis thaliana leaves. *Plant Physiology, 107*(4), 1129–1138.

Zeng, W., Lampugnani, E. R., Picard, K. L., Song, L., Wu, A. M., Farion, I. M., et al. (2016). Asparagus IRX9, IRX10, and IRX14A are components of an active xylan backbone synthase complex that forms in the Golgi apparatus. *Plant Physiology, 171*(1), 93–109.

Zhang, M., Li, Q., Kazachenko, A., & Xiang, Z. (2023). Crystallization and water cast film formability of birchwood xylans. *Cellulose, 30*(7), 4623–4638.

Zhao, X., Ouyang, K., Gan, S., Zeng, W., Song, L., Zhao, S., et al. (2014). Biochemical and molecular changes associated with heteroxylan biosynthesis in Neolamarckia cadamba (Rubiaceae) during xylogenesis. *Frontiers in Plant Science, 5*, 602.

Zhao, X., Tong, T., Li, H., Lu, H., Ren, J., Zhang, A., et al. (2017). Characterization of hemicelluloses from Neolamarckia cadamba (Rubiaceae) during xylogenesis. *Carbohydrate Polymers, 156*, 333–339.

Zheng, B., Yang, H., Xu, X., Xiang, Z., Hong, Z., Zheng, H., et al. (2023). Characterization of hemicellulose in Cunninghamia lanceolata stem during xylogenesis. *International Journal of Biological Macromolecules, 246*, Article 125530.

Zhong, R., Cui, D., Dasher, R. L., & Ye, Z. H. (2018). Biochemical characterization of rice xylan O-acetyltransferases. *Planta, 247*, 1489–1498.

Zhong, R., Cui, D., & Ye, Z. H. (2017). Regiospecific acetylation of xylan is mediated by a group of DUF231-containing O-acetyltransferases. *Plant and Cell Physiology, 58*(12), 2126–2138.